HHS Public Access

Author manuscript

Adv Funct Mater. Author manuscript; available in PMC 2020 May 21.

Published in final edited form as:

Adv Funct Mater. 2018 March 7; 28(10): . doi:10.1002/adfm.201704757.

High-Strength, Durable All-Silk Fibroin Hydrogels with Versatile Processability toward Multifunctional Applications

Zhenghua Zhu[†],
Department of Applied Engineering, Zhejiang Institute of Economic and Trade, Hangzhou, Zhejiang Province, 310018, China; Department of Biomedical Engineering, Tufts University, Medford, MA 02155, USA

Shengjie Ling[†],
Department of Civil and Environmental Engineering, Massachusetts Institute of Technology, Cambridge, MA 02139, USA; Department of Biomedical Engineering, Tufts University, Medford, MA 02155, USA; School of Physical Science and Technology, ShanghaiTech University, 393 Middle Huaxia Road, Shanghai 201210, China

Jingjie Yeo,
Department of Civil and Environmental Engineering, Massachusetts Institute of Technology, Cambridge, MA 02139, USA; Institute of High Performance Computing, A*STAR, 1 Fusionopolis Way, #16-16 Connexis, Singapore, 138632, Singapore

Siwei Zhao,
Department of Biomedical Engineering, Tufts University, Medford, MA 02155, USA; Department of Biomedical Engineering, Tufts University, Medford, MA 02155, USA

Lorenzo Tozzi,
Department of Biomedical Engineering, Tufts University, Medford, MA 02155, USA; Department of Biomedical Engineering, Tufts University, Medford, MA 02155, USA

Markus J. Buehler,
Department of Civil and Environmental Engineering, Massachusetts Institute of Technology, Cambridge, MA 02139, USA

Fiorenzo Omenetto,
Department of Biomedical Engineering, Tufts University, Medford, MA 02155, USA; Department of Biomedical Engineering, Tufts University, Medford, MA 02155, USA

Chunmei Li,
Department of Biomedical Engineering, Tufts University, Medford, MA 02155, USA; Department of Biomedical Engineering, Tufts University, Medford, MA 02155, USA

David L. Kaplan

david.kaplan@tufts.edu, chunmei.li@tufts.edu.
[†]These authors contributed equally to this work.

Supporting Information
Supporting Information is available from the Wiley Online Library or from the author.

Department of Biomedical Engineering, Tufts University, Medford, MA 02155, USA; Department of Biomedical Engineering, Tufts University, Medford, MA 02155, USA

Abstract

Hydrogels have been the focus of extensive research due to their potential use in fields including biomedical, pharmaceutical, biosensors, and cosmetics. However, the general weak mechanical properties of hydrogels limit their utility. Here, we generate pristine silk fibroin (SF) hydrogels with excellent mechanical properties via a binary solvent induced conformation transition (BSICT) strategy. In this method, the conformational transition of SF is regulated by moderate binary solvent diffusion and SF/solvent interactions. β-sheet formation serves as the physical crosslinks that connect disparate protein chains to form continuous 3D hydrogel networks, avoiding complex chemical and/or physical treatments. The Young's modulus of these new BSICT-silk fibroin hydrogels can reach up to 6.5±0.2 MPa, tens to hundreds of times higher than that of conventional hydrogels (0.01-0.1 MPa). These new materials filled the "empty soft materials space" in the elastic modulus/strain Ashby plot. More remarkably, the BSICT-SF hydrogels can be processed into different constructions through different polymer and/or metal based processing techniques, such as molding, laser cutting, and machining. Thus, these new hydrogel systems exhibit potential utility in many biomedical and engineering fields.

Keywords

high-strength hydrogel; silk; biomaterial; complex structure

1. Introduction

Hydrogels are usually considered a class of mechanically weak materials because of their solution-like nature, i.e. the low density of polymer chains and low friction between the chains.[1-4] In contrast, there are examples of biological hydrogels that exhibit excellent mechanical performance. For example, cartilage has high mechanical strength with excellent resilience to fulfill their multiple functions in the body.[5] Therefore, the challenge is to fill the gap in mechanical performance between man-made and biologically generated hydrogels. Recently, several robust synthetic hydrogels were prepared, such as double network hydrogels,[6-10] nanocomposite hydrogels,[11-15] and topological hydrogels,[16, 17] providing new approaches for hydrogel applications in the field of structural biomaterials. However, in practice, structural biomaterials not only require excellent mechanical properties but those with biocompatibility and controllable biodegradability are also in demand for medical and related applications. The poor biocompatibility and biodegradability of many of the synthetic hydrogels along with the potential toxicity of their degradation product hinder their applications in the medical field.[18-22]

Given the biocompatibility, biodegradability, and excellent mechanical properties of silk fibroin (SF), a protein derived from *Bombyx mori* (*B. mori*) cocoons, the fabrication of high mechanical performance SF hydrogels has been explored. However, most reported SF hydrogels remain weak and brittle, with poor load-bearing capabilities.[23,24] Although the addition of chemical and enzymatic cross-linking,[19, 25-27] and/or other synthetic polymers

can enhance the mechanical properties,[21] generating SF hydrogels with the combination of high strength and toughness while retaining full degradability and compatibility remains a challenge. Further, the additional chemical components usually give rise to potentially toxic and uncontrollable degradation products.[20] Therefore, a novel strategy for the formation of SF hydrogels that merge both mechanical and biological advantages is needed.

Here, we designed a binary solvent induced conformation transition (BSICT) strategy to produce pristine SF hydrogels with remarkable mechanical properties. In this approach, silk fibroin is first dissolved in hexafluoroisopropanol (HFIP, the first solvent) to obtain a homogeneous solution and then deionized (DI) water (the second solvent) is added to the solution to trigger the gel formation. The solvent-trigged method has been used to induce gelation for different aromatic peptide amphiphiles.[28] For example, the gelation of di-Fomoc-L-lysine in the mixture of various aprotic and polar solvents and water has been achieved.[29]

In contrast to previous methods to fabricate robust hydrogels,[30] the new BSICT strategy avoids complex chemical and/or physical treatments for hydrogel formation and does not require additional cross-linking agents and/or other chemical components to improve the mechanical properties. We also demonstrated that the BSICT-SF hydrogels displayed high mechanical performance that combines high strength and durability. These hydrogels showed significant improvement over previously reported SF hydrogels,[21,27] and the toughness are comparable with the previously reported highest value for biopolymer-based hydrogels (chemical and physical cross-linked cellulose hydrogels).[31] More remarkably, the combination of ease of fabrication and superior mechanical performance of those hydrogels allowed the use of versatile processing techniques to generate constructs with complex features which are rarely attained with the use of the previously produced robust hydrogels and the current hydrogel processing methods. These new systems are suitable for potential applications in structural biomaterials and in biomedical and engineering fields, such as for artificial blood vessels, protein chips, and soft robotics.

2. Results and discussion

Figure 1 is a schematic of the typical BSICT strategy used to fabricate high-strength SF hydrogels. Initially, aqueous SF solution (~6–8 wt%) was freeze-dried and then dissolved in HFIP to form a SF/HFIP solution. After the SF was completely dissolved, the desired volume of deionized (DI) water was gently dropped into the SF/HFIP solution. After mixing, a transparent SF/HFIP/H_2O solution was obtained (Figure S1). The resultant solution was then transferred into a covered bottle and incubated at various temperatures until protein gelation. Finally, the SF hydrogel was washed thoroughly with DI water to remove HFIP solvent via solvent-exchange and solvent evaporation. The removal of the HFIP solvent in SF hydrogels was confirmed by FTIR (Figure S2).

SF concentration plays a critical role in BSICT-SF hydrogel formation. In initial experiments, the H_2O/HFIP volume ratio was fixed at 1.5:3 v/v and no hydrogel formed over 10 days when the SF/HFIP ratio was lower than 0.2:3 w/v. Increasing the SF/HFIP ratio to 0.45:3 w/v (weight-to-volume ratio of 15%), a uniform hydrogel formed in 2 days.

Accordingly, in consideration of the SF solubility in HFIP as well as the gelation rate, the SF/HFIP ratio was fixed at 15% w/v in all subsequent experiments. It is worth noting that the order in which solvents are added cannot be changed. The other three possible orders that solvents can be added, i.e., either adding SF/HFIP solution into water, adding SF aqueous solution into HFIP, or adding HFIP into SF aqueous solution, do not result in the formation of a uniform hydrogel, instead they form precipitates and heterogeneous hydrogels (Figure. S3). The H_2O/HFIP volume ratio is another crucial factor for BSICT-SF hydrogel formation. No hydrogels were formed even after 5 days of incubation if 0.6 ml of DI water was added to a SF/HFIP solution with the starting volume and weight-and-volume ratio of 3 ml and 15% w/v, respectively. On the other hand, if the amount of DI water added was increased to 1.2 ml, uniform hydrogels formed in 3 days (Table 1 and Figure 2a). On the basis of these initial findings, we systematically investigated the effects of H_2O/HFIP volume ratio on BSICT-SF gelation (Table 1). By increasing the H_2O/HFIP volume ratio from 1:5 to 1.1:1, the gelation rate increased gradually and the resultant hydrogels (discs of 20 mm diameter and 10 mm thickness) changed from semi-transparent to white with pore sizes changed from 100–500 nm to 2–5 μm (Figure 2b,c). Another important factor that affects hydrogel formation is temperature. Hydrogels of formula sample 4 were formed at room temperature, 37 °C and 48 °C. The gelation time of SF decreased with increase in the temperature, and the gelation time at room temperature, 37 °C and 48 °C was 2 days, 2 hours and 1 hour, respectively. With the increase of temperature, interaction among the SF chains increases, leading to the formation of higher number of nucleation seeds to facilitate the hydrogel formation. In addition, the transparency of the resulting hydrogels increased with the increase of temperature (Figure S4). This could be ascribed to the smaller size of the β-sheet crystallites formed at higher temperature. It was also observed that SF hydrogels formed at different temperatures had similar loading-unloading curves and good fatigue resistance after the first cycle.

To elucidate the BSICT-SF gelation mechanism, replica-exchange molecular dynamics (REMD) simulations were performed,[32] which have been widely used for the study of conformational equilibria in proteins. With this method, non-interacting replicas of the molecular system were simulated simultaneously at different temperatures. Exchange of neighboring replicas at regular intervals reduced trapping in local energy minima and improves phase space sampling of protein conformations. Thus, by comparing the results from two different solvents and the co-solvent systems (Figure 3a-c and Figure S5a-c), differences in SF solvation mechanisms between the two solutions and in co-solvent can be identified. The REMD simulations with solute tempering (REST)[33-35] revealed that in the five most populated clusters (Figure 3a-c), randomly dispersed SF chains were able to spontaneously form approximately 6.0% of β-sheets when solvated in pure HFIP (Figure 3b,d) whereas solvation in pure water only led to the formation of mostly amorphous aggregates with approximately 3.1% β-sheet (Figure 3a,d).

These results verify previous circular dichroism assessments of SF in SF/HFIP solution that SF was predominantly helical structures with some β-sheet content, whereas SF in water adopted random coil conformations.[36] The low dielectric constant of HFIP (16.7 at 298.2K) effectively aids in hydrogen bond formation between strands of SF, whereas water shields these electrostatic interactions due to its high dielectric constant (78.3 at 298.2K).[37]

This factor led to a 17% increase in the number of intra-protein hydrogen bonds in HFIP in comparison with solvation in water (Figure 3d). Thereafter, β-sheet formation accelerated as water was slowly mixed with SF/HFIP system. Water molecules displace the HFIP molecules and yet they do not destabilize the β-sheets that were already present in the SF. β-sheet content rose to 7.5% after REST (Figure 3c,d). Concurrently, the number of intra-protein hydrogen bonds rose dramatically by almost 40% (Figure 3e), indicating that further β-sheet formation was likely. However, due to time constraints inherent to classical molecular dynamics simulations, the gelation kinetics of silk over the period of days cannot be probed. In addition, conventional molecular dynamics simulations over 20ns also show that high concentrations of water strongly destabilized the predominantly helical structures of silk in HFIP (Figure S5d,e), leading to further opportunities for β-sheet growth from the initial seeds to induce gelation.

Therefore, by tuning the concentration at which water is introduced as a co-solvent, further β-sheet formation is accelerated through the growth of initial seeds when solvated in HFIP. This allows the gelation of the hydrogel, as demonstrated in the experimental results, due to the fact that the silk domains that form β-sheets are hydrophobic and insoluble in water. Higher amounts of β-sheet and intra-protein hydrogen bonds form when silk is solvated in HFIP at higher concentration, providing more initial nucleation seeds for further β-sheet formation after water is introduced as a co-solvent. This allows the faster gelation of SF hydrogel, as demonstrated by experimental results. These simulations also show the rationale behind the critical role of the order in which each solvent is added. Pure HFIP is required to solvate the SF while providing the initial seeds of β-sheets. Subsequently, water is introduced to the system and rapidly increases the rate of β-sheet formation by promoting hydrogen bonds between the protein chains, thereby inducing gelation as HFIP molecules mix with water molecules. This sequence also explains why increasing the concentration of water significantly accelerated the gelation process.

Visual images of BSICT-SF hydrogels are presented in Figure 2d. Different 3D shapes (e.g., polygon, sphere, tube, cone, cylinder) with different material formats (e.g., film, tube, bulk material) were fabricated and they appeared homogenous, freestanding and devoid of cracks. The colors can be easily changed via mixing with different organic and inorganic dyes.[38-41] For instance, the red SF hydrogels were prepared by adding Rhodamine B into the water solution. Since SF is an amphiphilic polymer that consists of alternating hydrophobic and hydrophilic domains, it strongly binds some different types of dyes. Furthermore, the transparency of the hydrogels increased with a decrease of hydrogel thickness. A 2 mm-thick hydrogel of sample 4 was transparent under visible light (Figure 2f), in contrast to the white color observed with traditional SF hydrogels prepared by alcohol, heating, or ultrasonic treatments (Figure S6a). To quantitatively evaluate the transmittance of BSICT-SF hydrogel membranes, 400 μm thick hydrogels were characterized via a fiber-optic spectrometer (Figure S7 and Table 1). The hydrogels of samples 2–4 were optically transparent (above 61% transmission) throughout the visible region (350–800 nm), and up to ~90% at 800 nm. These transmission values were comparable with the as-cast (90% at 800 nm) and higher than ethanol-treated (77% at 800 nm) SF membranes (Figure S7) with similar thickness and comparable with transparent polymeric membranes prepared from polycarbonate (89%) and poly(methyl methacrylate) (92%).[42]

Additionally, in contrast to traditional 10 wt% SF hydrogels which are brittle and break easily (Figure S6b), the BSICT-SF hydrogels were robust, flexible, and able to bend, be tied into knots and cut (Figure 2g,h). The gels also exhibited good elasticity; for example, a BSICT-SF hydrogel ball was used in a game of table tennis and bounced like a traditional table tennis ball without rupturing (Figure 2i). This response demonstrated the ability of the hydrogel to retain mechanical properties after deformation. This is a remarkable feature for biopolymer hydrogels because most biopolymer hydrogels lack flexibility and elasticity. Similar behavior was only achieved in double-cross-linked (covalent cross-linking and physical cross-linking) cellulose hydrogels.[31] BSICT-SF hydrogels do not have any covalent cross-links, thus all of these outstanding mechanical behaviors are derived directly from the internal hydrogen bonds and β-sheets. These structures act as crosslinks to form interlocking protein chains that ensure the SF molecules are stable in the hydrogels. To assess β-sheet content, the freeze-dried BSICT-SF hydrogel samples were characterized by Fourier transform infrared (FTIR) spectroscopy (Figure S8). The deconvolution of the amide I band provides[43,44] an estimate of the percentage of β-sheets in the hydrogels of ~35% (Table 1 and Figure S7b), while the SF hydrogel formed by 70% v/v ethanol solution treatment was 40±1% (Figure S7c). High β-sheet content usually leads to lower strength and toughness in protein-based materials. For instance, *B. mori* silkworm silk fiber has higher β-sheet content (37–56%)[45-47] than spider major ampullate silk (11–15%),[43,48] but it is weaker and less extensible than spider major ampullate silk.[49] Moreover, moderate β-sheet content helps to provide a good balance in strength and elasticity of a material. This is also a reason why silkworm silk can usually be either strong or elastic with variations in the spinning condition, whereas spider silk combines both properties under different spinning conditions.[49]

The contributions of internal hydrogen bonds and β-sheets cannot be quantified separately as the formation of β-sheets also rests upon the formation of hydrogen bonds. However, the impact of increasing amounts of β-sheets can be quantitatively analyzed numerically. We performed additional computational simulations based on the Dissipative Particle Dynamics (DPD) model derived previously for silks.[50] DPD is a coarse-grained particle-based modelling technique for mesoscale simulations of materials.[51] Based on this technique, bead-spring models are generated with interaction terms that represent the hydrophobic and hydrophilic regions in linear chains of silk, as well as hydrogen bonding which leads to β-sheet formation. We performed uniaxial tensile tests after generating equilibrated silk chains that have hydrophobic to hydrophilic bead ratios of 1:1, 4:1, and 9:1, which represent increasing amounts of β-sheets relative to the hydrophilic linkers. From Figure S9, on the one hand, we can see that excessively low amounts of β-sheets will result in a gel that is unable to take any load, where the chains are just sliding against each other. On the other hand, excessively large amounts of β-sheets will result in a very brittle response. Therefore, it is clear that the gel requires a moderate amount of β-sheets in order to have the excellent mechanical response as shown in our experiments.

The mechanical properties of the BSICT-SF hydrogels were systematically evaluated under tension and compression loading. The representative stress-strain curves of tensile testing are plotted in Figure 4a and the mechanical properties summarized in Table S1. When the SF solid content was increased (from sample 9 of 8.3±0.3 to sample 2 of 14.0±0.4 wt%), the

failure strength of the hydrogels increased from 0.08±0.02 to 0.70±0.04 MPa. The compression stress-strain curves of four samples in different batches almost coincided (Figure 4d), confirming the repeatability of a given gelation condition. Surprisingly, a BSICT-SF hydrogel with a thickness of 1 mm had a Young's modulus of 6.5±0.2 MPa (sample 2 with a water content 86.0±0.4 wt%), tens to hundreds of times higher than that of conventional hydrogels (0.01–0.1 MPa).[18] These values were also significantly higher than natural cartilage (0.45–0.8 MPa),[8,52] most double-network synthetic hydrogels (0.1–1 MPa),[53,54] other recently reported high-performance biopolymer hydrogels, such as chemical and physical cross-linked chitin hydrogels (0.05–0.26 MPa),[55] horseradish peroxidase and alcohol cross-linked SF hydrogels (0.31–3.0 MPa),[27] and SF/hydroxypropyl methyl cellulose hydrogels (0.37–1.23 MPa).[21] The values are comparable with chemical and physical cross-linked cellulose hydrogels (0.2–4.9 MPa).[31] In terms of hydrogel toughness, as reflected in the work of extension at fracture, the BSICT-SF hydrogels (sample 4) had values of 0.60±0.09 MJ m^{-3}, comparable to the highest value for biopolymer based hydrogels (chemical and physical cross-linked cellulose hydrogels (0.65 MJ m^{-3}).[31]

According to the findings of Miserez et al.,[56] when drawing an elastic modulus/strain Ashby plot of the most commonly used biopolymer hydrogels and other "soft" biomaterials (Figure. 4g), these materials are mostly segregated into two broad classes. They are either elastically stretchable with limited modulus, such as alginate and double network hydrogels, or they are stiff with very low failure strains, as in the case of native collagen. Few "soft" biomaterials (most are hydrogels) have elastic moduli in the range of 1–100 MPa, and this range has been aptly termed as the "empty soft materials space". This conclusion implies that "soft" materials are limited in attaining the combination of mechanical properties in this space. However, the BSICT-SF hydrogels fill this empty "soft" material space beautifully. They expand the range of existing biomaterials and enhanced both stiffness and extensibility.

For practical applications, structural biomaterials not only require high modulus and fracture toughness, but they also need to have high deformation and energy dissipation. We performed loading-unloading tests at a strain of 20% to evaluate the self recovery of the BSICT-SF hydrogels under both tensile and compressive conditions. It was observed that the BSICT-SF hydrogel had better self-recovery property under tension than compression and the recovery depended on the resting time between cycles (Figure 4b and e). When the second test was conducted immediately, the hydrogel under tension recovered to 99% of its original length and the dissipated energy recovered to 33% of its original value. When the second loading cycle was conducted after 60 minutes, the sample almost recovered to its original length and the dissipated energy recovered to 61% of its original value. The results demonstrated that the internal network damage caused by mechanical testing could be better recovered by prolonging the resting time before reloading. The less recovery of the hydrogel under compressive loading seemed to be the loss of water from the gel during the initial compression loading. It was reported that water has a healing effect on hydrogels under cyclic compression.[57] We also observed that BSICT-SF hydrogel demonstrated apparent hysteresis loops, indicating that energy dissipation was effective during the loading-unloading cycles. The hydrogel absorbed more than 60% energy at a strain of 20% under tensile and compressive loading, which occupies the empty soft material space in the

hysteresis/elastic modulus Ashby plot (Figure 4h). Clearly, the BSICT-SF hydrogels expand the range of existing material mechanical properties for a wide range of potential regenerative medical applications. The mechanical performance of the BSICT-SF hydrogels was even more remarkable under loading-unloading cycles at varying maximum tension and compression without applying resting between any two consecutive cycles (Figure 4c and f). The BSICT-SF hydrogels showed pronounced hysteresis after unloading, and the stress and hysteresis loop of the hydrogels increased gradually with applied strain (Figure 4c and f, insets). Furthermore, for each strain value, the loading-unloading cycles showed that very little plastic deformation or strength degradation occurred in the BSICT-SF hydrogels after the first cycle, indicating the good shape recovery properties and fatigue resistance after the first cycle.

The BSICT-SF hydrogel network is physically crosslinked by internal hydrogen bonds and β-sheet structures. The β-sheet structures may exist in silk hydrogels in two different forms: crystallite-forming β-sheets and the non crystallite-forming β-sheets. When the tensile or compressive loading was applied on the BSICT-SF hydrogels, the hydrogen bonds could serve as reversible sacrificial bonds to dissipate energies, while the β-sheet crystallites may act as stress transfer centers to effectively adsorb energy and withstand deformation. The recovery behavior after the first cycle could be attributed to the reversible characteristic of the physically crosslinked silk fibroin network, especially the β-sheet crystallites within the hydrogels. In addition, the nanofibrous/nanoporous structure of the hydrogel itself (Figure S10) could effectively transfer mechanical stress. On the one hand, the intertwined nanofibers could transfer energy via the hydrogen bonding interaction between the silk fibroin fibers. On the other hand, the nano-sized pores could distribute stress more evenly to resistant stress concentration and the small pore size and increased number of pores also act as a barrier against crack propagation.[58]

Hydrogels with complex structures have implication in many bio-related applications. For example, hydrogel scaffolds with complex internal and external architectures that mimic the native tissue structure are expected to outperform those with uncontrolled structures. We next explored the processability of this class of newly developed silk hydrogels into functional formats with sophisticated features. Due to the moderate and controllable sol-gel transition process, BSICT-SF hydrogels can be constructed as polymorphic structures, thus moving beyond bulk features, via reverse molding methods. A typical route of fabricating channeled BSICT-SF hydrogel devices is illustrated in Figure 5a. Briefly, a solid paraffin pattern was created by a solution molding method and then immersed into the SF/HFIP/H_2O solution. After the sol-gel transition, a BSICT-SF hydrogel took the shape of the solid paraffin pattern and was then transferred into DI water (~80 °C) to remove the paraffin. Finally, a channeled BSICT-SF hydrogel was harvested by thoroughly washing away the residual HFIP. The resultant hydrogel replicated the tortuous and interconnected pattern with a sharp boundary (Figure 5b-d). A channeled hydrogel was also fabricated by sequential deposition of three hydrogels layers. The uniform structure of the cross-section (Figure 5d) demonstrated the good bonding between adjacent layers and allowed the layer-by layer fabrication of 3D channels. This facile approach offers new opportunities for developing SF microfluidic chips with excellent mechanical performance that can accelerate the development of on-chip cell sensing systems. In addition, micro/nano-molding technique

was used to generate hydrogel patterns of micro- and nano-size topography. For example, pattern of ~450 nm gratings was successfully achieved on BSICT-SF hydrogel via simple casting the hydrogel on PDMS molds (Figure 5e). The human umbilical vein endothelial cells (HUVECs) seeded on the patterned hydrogels formed confluent cell monolayer while maintaining their phenotype by expressing the endothelial marker CD31 (Figure 5f and Figure S11b). In contrast, only isolated cell patches formed on unpatterned flat hydrogels (Figure S11a). The patterned BSICT-SF hydrogel surface provided structural cues to influence cell behavior, suggesting their potential use in biomedical field.

The exceptional mechanical properties of the BSICT-SF hydrogels allowed them to undergo more extreme processing techniques, such as laser cutting (Figure 5g) and machining (Figure 5l), which are usually used for metal and/or polymer processing. Figure 5h shows a BSICT-SF hydrogel being cut by laser. Different words and sophisticated patterns were directly “written” on the hydrogels. The written depth was tunable by controlling the laser intensity, where the penetrating (Figure 5i) and semi-closed patterns (Figure 5j) were obtained. The patterned hydrogel was strong and flexible and no burning and breakage of the hydrogel was observed (Figure S12). The 260 μm wide lines at the connection point of the word “f” and “t” are intact (Figure 5i), indicating that the processing resolution of BSICT-SF hydrogels can be as small as 260 μm. Furthermore, different functional patterns were achieved via laser cutting (Figure. 5k). A representative example is an auxetic structure, which is a mechanical metastructure that has a negative Poisson’s ratio; when materials with auxetic structures are stretched, they become thicker in the dimension perpendicular to the applied force. This occurs due to their particular internal structure and the way this structure deforms when the sample is loaded uniaxially. These particular structures and materials have shown a wide range of applications in tissue engineering and biosensors. Figure 5k demonstrates significant auxetic deformation of a reentrant honeycomb BSICT-SF hydrogel fabricated by laser cutting. In practice, laser cutting is suitable for cutting 2D patterns, while machining techniques are more useful for processing 3D structures. Therefore, we further explored the machinability of BSICT-SF hydrogels. As shown in Figure 5m, an “L” shaped channel was drilled into a bulk BSICT-SF hydrogel by a machining drill bit. Sharp, smooth, and uniform sawtooth threads with a thread pitch of 800 μm were observed on the internal surface of the channel. Additionally, a hydrogel screw was successfully machined from BSICT-SF blank hydrogels (Figure 5n). A glossy structure without any defects was formed, while distinct threads with clear edges were found. The SEM images revealed that the screw had a dense surface (Figure 5o) and porous interior (Figure 2b), which shows potential for producing lightweight materials. The universal processing capabilities of BSICT-SF hydrogels combined with their good cell compatibility further endowed their potential for developing advanced functional materials, such as artificial cartilage, microfluidics chip, and soft sensors and robots.

3. Conclusion

In summary, we developed a novel BSICT approach to fabricate high-strength, durable all-silk fibroin hydrogel, in which solvent diffusion -induced conformational transitions were adopted to trigger and regulate SF gelation. In this process, the SF transitioned from random coils and/or helical structures to β-sheets, which directly served as physical crosslinks. This

avoided the introduction of extremely complicated physical and chemical gel reactions, thus maintaining the simplicity of the design. Meanwhile, the BSICT gelation rates were tunable within a time frame of 1–3 days. More importantly, the resultant BSICT-SF hydrogels possessed strong mechanical properties that combined high strength and toughness, and also exhibited utility with multiple processing techniques, including laser cutting and turning. This facile SF hydrogel formation strategy is also suitable for other proteins, such as bovine serum albumin (BSA) and soy protein isolate (SPI) (Figure S13). As a general protein hydrogel fabrication method, the BSICT shows promising utility towards new materials for biomedicine, engineering and soft robotics.

4. Experimental Section

BSICT strategy for making tough all-SF hydrogels:

BSICT strategy for making tough all-SF hydrogels. Lyophilized silk was prepared from the cocoons of the silk worm *Bombyx mori* as previously described.[57] Silk/HFIP solution was generated by dissolving lyophilized silk in HFIP. To prepare the BSICT hydrogel, desired volumes of DI water were slowly dropped into a 3 ml 15% w/v SF/HFIP solution, followed by thorough mixing by gentle rotation. The resultant solutions were transferred into a glass bottle, sealed and incubated for several days toward SF gelation. The solutions required static incubation as any disturbance may prolong the gelation and lead to inhomogeneity in hydrogel structure. Finally, the as-formed hydrogels were washed with DI water at 100 °C for several rounds (around 2 hours) to thoroughly remove residual HFIP via solvent-exchange and solvent evaporation.

Details on the experimental methods, molecular dynamics simulation[32-35, 60-72] and the characterization of the morphological, physical, chemical, and mechanical properties of the BSICT hydrogel may be found in Supporting information.

Supplementary Material

Refer to Web version on PubMed Central for supplementary material.

Acknowledgements

We acknowledge Harvard University Center for Nanoscale Systems (CNS) for providing AFM and SEM measurements. The CNS is a member of the National Nanotechnology Coordinated Infrastructure Network (NNCI), which is supported by the National Science Foundation under NSF award no. 1541959. Computational simulations were performed on the Extreme Science and Engineering Discovery Environment (XSEDE), which is supported by the National Science Foundation grant number ACI-1053575, and Singapore's A*STAR Computational Resource Centre and National Supercomputing Centre. This work was supported by China Scholarship Council (CSC), the NIH (R01EB021264, U01EB014976, R01DE016525), and Zhejiang Provincial Natural Science Foundation (Y14C100005), and with additional support provided by ONR (N00014–16-1–2333 and N000141612333), AFOSR (FA9550–11-1–0199, FA9550–14-1–0015, FA8650–16-C-5020), and the NSF IGERT program.

References

[1]. Tanaka Y, Gong JP, Osada Y, Prog. Polym. Sci 2005, 30, 1.

[2]. Du X, Zhou J, Shi J, Xu B, Chem. Rev 2015, 115, 13165. [PubMed: 26646318]

[3]. Van Vlierberghe S, Dubruel P, Schacht E, Biomacromolecules 2011, 12, 1387. [PubMed: 21388145]

[4]. Buwalda SJ, Boere KWM, Dijkstra PJ, Feijen J, Vermonden T, Hennink WE, J. Control. Release 2014, 190, 254. [PubMed: 24746623]

[5]. Abé H, Hayashi K, M. S. Ph D., Data Book on Mechanical Properties of Living Cells, Tissues, and Organs, Springer, 1996.

[6]. Yuk H, Zhang T, Lin S, Parada GA, Zhao X, Nat Mater 2016, 15, 190. [PubMed: 26552058]

[7]. Gong JP, Katsuyama Y, Kurokawa T, Osada Y, Adv. Mater 2003, 15, 1155.

[8]. Gong JP, Soft Matter 2010, 6, 2583.

[9]. Mredha MTI, Kitamura N, Nonoyama T, Wada S, Goto K, Zhang X, Nakajima T, Kurokawa T, Takagi Y, Yasuda K, Gong JP, Biomaterials 2017, 132, 85. [PubMed: 28411451]

[10]. Nonoyama T, Wada S, Kiyama R, Kitamura N, Mredha MTI, Zhang X, Kurokawa T, Nakajima T, Takagi Y, Yasuda K, Gong JP, Adv. Mater 2016, 28, 6740. [PubMed: 27184968]

[11]. Liu M, Ishida Y, Ebina Y, Sasaki T, Hikima T, Takata M, Aida T, Nature 2015, 517, 68. [PubMed: 25557713]

[12]. Wang Q, Mynar JL, Yoshida M, Lee E, Lee M, Okuro K, Kinbara K, Aida T, Nature 2010, 463, 339. [PubMed: 20090750]

[13]. Haraguchi K, Takehisa T, Adv. Mater 2002, 14, 1120.

[14]. Haraguchi K, Ebato M, Takehisa T, Adv. Mater 2006, 18, 2250.

[15]. Haraguchi K, Curr. Opin. Solid State Mater. Sci 2007, 11, 47.

[16]. Okumura Y, Ito K, Adv. Mater 2001, 13, 485.

[17]. Oku T, Furusho Y, Takata T, Angew. Chem., Int. Ed 2004, 43, 966.

[18]. Li J, Illeperuma WRK, Suo Z, Vlassak JJ, ACS Macro Lett. 2014, 3, 520.

[19]. Partlow BP, Hanna CW, Rnjak-Kovacina J, Moreau JE, Applegate MB, Burke KA, Marelli B, Mitropoulos AN, Omenetto FG, Kaplan DL, Adv. Funct. Mater 2014, 24, 4615. [PubMed: 25395921]

[20]. Zhao Y, Nakajima T, Yang JJ, Kurokawa T, Liu J, Lu J, Mizumoto S, Sugahara K, Kitamura N, Yasuda K, Daniels AUD, Gong JP, Adv. Mater 2014, 26, 436. [PubMed: 24431128]

[21]. Luo K, Yang Y, Shao Z, Adv. Funct. Mater 2016, 26, 872.

[22]. Gonzalez MA, Simon JR, Ghoorchian A, Scholl Z, Lin S, Rubinstein M, Marszalek P, Chilkoti A, López GP, Zhao X, Adv. Mater 2017, 29, 1604743.

[23]. Kapoor S, Kundu SC, Acta Biomater. 2016, 31, 17. [PubMed: 26602821]

[24]. Vepari C, Kaplan DL, Prog. Polym. Sci 2007, 32, 991. [PubMed: 19543442]

[25]. Vasconcelos A, Gomes AC, Cavaco-Paulo A, Acta Biomater. 2012, 8, 3049. [PubMed: 22546517]

[26]. Whittaker JL, Choudhury NR, Dutta NK, Zannettino A, J. Mater. Chem. B 2014, 2, 6259. [PubMed: 32262143]

[27]. Su D, Yao M, Liu J, Zhong Y, Chen X, Shao Z, ACS Appl. Mater. Interfaces 2017, 9, 17489. [PubMed: 28470062]

[28] a). Chen L, Raeburn J, Sutton S, Spiller DG, Williams J, Sharp JS, Griffiths PC, Heenan RK, King SM, Paul A, Furzeland S, Atkins D, Adams DJ, Soft Matter 2011, 7, 9721;b)Raeburn J, Mendoza-Cuenca C, Cattoz BN, Little MA, Terry AE, Zamith Cardoso A, Griffiths PC, Adams DJ, Soft Matter 2015, 11, 927; [PubMed: 25516486] c)Ryan DM, Anderson SB, Nilsson BL, Soft Matter 2010, 6, 3220;d)Zhang Y, Li S, Ma M, Yang M, Wang Y, Hao A, Xing P, New J. Chem 2016, 40, 5568;e)Zhu P, Yan X, Su Y, Yang Y, Li J, Chem. Eur. J 2010, 16, 3176. [PubMed: 20119986]

[29]. Hashemnejad SM, Huda MM, Rai N, Kundu S, ACS Omega 2017, 2, 1864. [PubMed: 31457548]

[30]. a) Chen Q, Chen H, Zhu L, Zheng J, J. Mater. Chem. B 2015, 3, 3654; [PubMed: 32262840] b) Xu D, Huang J, Zhao D, Ding B, Zhang L, Cai J, Adv. Mater 2016, 28, 5844; [PubMed: 27158931] c) Hu X, Vatankhah-Varnoosfaderani M, Zhou J, Li Q, Sheiko SS, Adv. Mater 2015, 27, 6899 [PubMed: 26436409]

[31]. Zhao D, Huang J, Zhong Y, Li K, Zhang L, Cai J, Adv. Funct. Mater 2016, 26, 6279.

[32]. Sugita Y, Okamoto Y, Chem. Phys. Lett 1999, 314, 141.

[33]. Liu P, Kim B, Friesner RA, Berne BJ, Proc. Natl. Acad. Sci. U. S. A 2005, 102, 13749. [PubMed: 16172406]

[34]. Wang L, Friesner RA, Berne BJ, J. Phys. Chem. B 2011, 115, 9431. [PubMed: 21714551]

[35]. Jo S, Jiang W, Comput. Phys. Commun 2015, 197, 304.

[36]. Trabbic KA, Yager P, Macromolecules 1998, 31, 462.

[37]. Wohlfarth C, Static dielectric constants of pure liquids and binary liquid mixtures, Springer Berlin Heidelberg, 2008.

[38]. Ling S, Li C, Jin K, Kaplan DL, Buehler MJ, Adv. Mater 2016, 28, 7783. [PubMed: 27352291]

[39]. Ling S, Zhang Q, Kaplan DL, Omenetto F, Buehler MJ, Qin Z, Lab Chip 2016, 16, 2459. [PubMed: 27241909]

[40]. Iizuka T, Sezutsu H, Tatematsu K.-i., Kobayashi I, Yonemura N, Uchino K, Nakajima K, Kojima K, Takabayashi C, Machii H, Yamada K, Kurihara H, Asakura T, Nakazawa Y, Miyawaki A, Karasawa S, Kobayashi H, Yamaguchi J, Kuwabara N, Nakamura T, Yoshii K, Tamura T, Adv. Funct. Mater 2013, 23, 5232.

[41]. Tansil NC, Li Y, Teng CP, Zhang S, Win KY, Chen X, Liu XY, Han M-Y, Adv. Mater 2011, 23, 1463. [PubMed: 21433114]

[42]. Mark JE, Polymer data handbook, Oxford university press, 2009.

[43]. Ling S, Qi Z, Knight DP, Shao Z, Chen X, Biomacromolecules 2011, 12, 3344. [PubMed: 21790142]

[44]. Ling S, Qi Z, Knight DP, Huang Y, Huang L, Zhou H, Shao Z, Chen X, Biomacromolecules 2013, 14, 1885. [PubMed: 23607809]

[45]. Tanaka C, Takahashi R, Asano A, Kurotsu T, Akai H, Sato K, Knight DP, Asakura T, Macromolecules 2008, 41, 796.

[46]. Martel A, Burghammer M, Davies RJ, Riekel C, Biomacromolecules 2007, 8, 3548. [PubMed: 17949104]

[47]. Drummy LF, Farmer BL, Naik RR, Soft Matter 2007, 3, 877.

[48]. Grubb DT, Jelinski LW, Macromolecules 1997, 30, 2860.

[49]. Romer L, Scheibel T, Prion 2008, 2, 154. [PubMed: 19221522]

[50]. a) Dinjaski N, Ebrahimi D, Qin Z, Giordano JEM, Ling S, Buehler MJ, Kaplan DL, J. Tissue Eng. Regen. Med 2016, DOI: 10.1002/term.2380;b) Jacobsen MM, Tokareva OS, Ebrahimi D, Huang W, Ling S, Dinjaski N, Li D, Simon M, Staii C, Buehler MJ, Kaplan DL, Wong JY, Macromol. Biosci 2017, 17;c) Lin S, Ryu S, Tokareva O, Gronau G, Jacobsen MM, Huang W, Rizzo DJ, Li D, Staii C, Pugno NM, Wong JY, Kaplan DL, Buehler MJ, Nat. Comm 2015, 6, 6892;d) Ling S, Li C, Jin K, Kaplan DL, Buehler MJ, Adv. Mater 2016, 28, 7783; [PubMed: 27352291] e) Rim NG, Roberts EG, Ebrahimi D, Dinjaski N, Jacobsen MM, Martin-Moldes Z, Buehler MJ, Kaplan DL, Wong JY, ACS Biomater. Sci. Eng 2017, 3, 1542. [PubMed: 28966980]

[51]. Groot RD, Warren PB, J. Chem. Phys 1997, 107, 4423.

[52]. Mansour MJ, in Kinesiology: The Mechanics and Pathomechanics of Human Movement 2003.

[53]. Nakajima T, Furukawa H, Tanaka Y, Kurokawa T, Osada Y, Gong JP, Macromolecules 2009, 42, 2184.

[54]. Gong JP, Soft Matter 2010, 6, 2583

[55]. Xu D, Huang J, Zhao D, Ding B, Zhang L, Cai J, Adv. Mater 2016, 28, 5844. [PubMed: 27158931]

[56]. Miserez A, Weaver JC, Chaudhuri O, J. Mater. Chem. B 2015, 3, 13. [PubMed: 32261919]

[57]. Harrass K, Kruger R, Moller M, Albrechtb K, Groll J, Soft Matter 2013, 9, 2869

[58]. Kim U-J, Park J, Li C, Jin H-J, Valluzzi R, Kaplan DL, Biomacromolecules 2004, 5, 786. [PubMed: 15132662]

[59]. Rockwood DN, Preda RC, Yucel T, Wang X, Lovett ML, Kaplan DL, Nat. Protoc 2011, 6, 1612. [PubMed: 21959241]

[60]. Best RB, Zhu X, Shim J, Lopes PEM, Mittal J, Feig M, MacKerell AD, J. Chem. Theory Comput 2012, 8, 3257. [PubMed: 23341755]

[61]. Phillips JC, Braun R, Wang W, Gumbart J, Tajkhorshid E, Villa E, Chipot C, Skeel RD, Kalé L, Schulten K, J. Comput. Chem 2005, 26, 1781. [PubMed: 16222654]

[62]. Vanommeslaeghe K, Hatcher E, Acharya C, Kundu S, Zhong S, Shim J, Darian E, Guvench O, Lopes P, Vorobyov I, Mackerell AD, J. Comput. Chem 2010, 31, 671. [PubMed: 19575467]

[63]. Mayne CG, Saam J, Schulten K, Tajkhorshid E, Gumbart JC, J. Comput. Chem 2013, 34, 2757. [PubMed: 24000174]

[64]. Martyna GJ, Tobias DJ, Klein ML, J. Chem. Phys 1994, 101, 4177.

[65]. Feller SE, Zhang Y, Pastor RW, Brooks BR, J. Chem. Phys 1995, 103, 4613.

[66]. Essmann U, Perera L, Berkowitz ML, Darden T, Lee H, Pedersen LG, J. Chem. Phys 1995, 103, 8577.

[67]. Martínez L, Andrade R, Birgin EG, Martínez JM, J. Comput. Chem 2009, 30, 2157. [PubMed: 19229944]

[68]. Humphrey W, Dalke A, Schulten K, J. Mol. Graph 1996, 14, 33. [PubMed: 8744570]

[69]. Daura X, Gademann K, Jaun B, Seebach D, van Gunsteren WF, Mark AE, Angew. Chem., Int. Ed 1999, 38, 236.

[70]. Abraham MJ, Murtola T, Schulz R, Páll S, Smith JC, Hess B, Lindahl E, SoftwareX 2015, 1–2, 19.

[71]. Joosten RP, te Beek TAH, Krieger E, Hekkelman ML, Hooft RWW, Schneider R, Sander C, Vriend G, Nucleic Acids Res. 2011, 39, D411. [PubMed: 21071423]

[72]. McGibbon Robert T., Beauchamp Kyle A., Harrigan Matthew P., Klein C, Swails Jason M., Hernández Carlos X., Schwantes Christian R., Wang L-P, Lane Thomas J., Pande Vijay S., Biophys. J 2015, 109, 1528. [PubMed: 26488642]

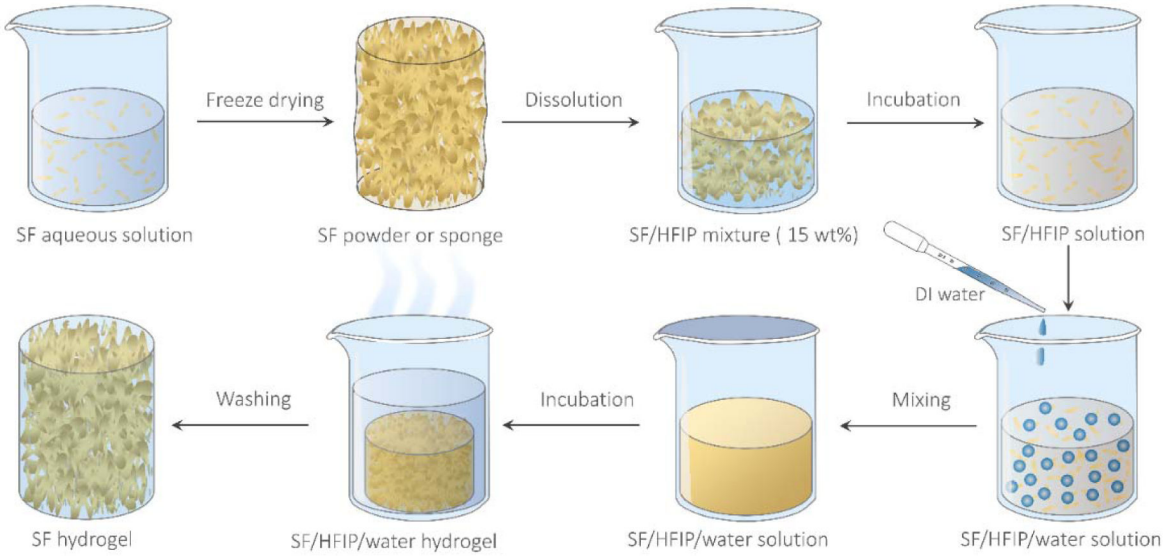

Figure 1.

Scheme of the BSICT strategy to fabricate pristine SF hydrogels with high mechanical performance.

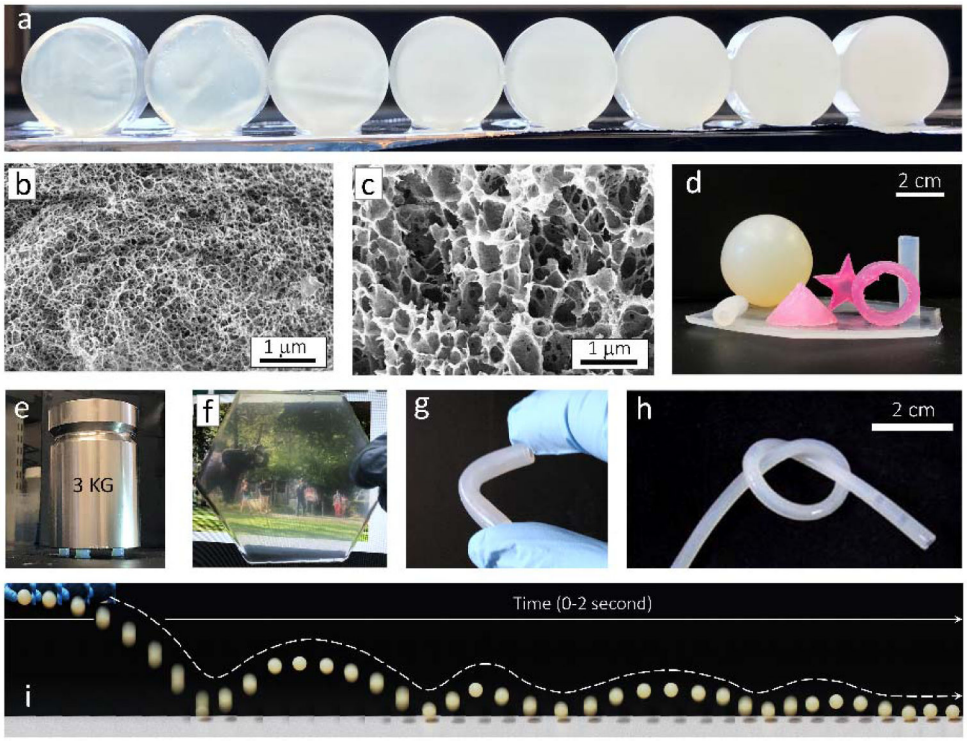

Figure 2.

Visual appearance and structural characterization of the BSICT hydrogels. a) Digital photo of the BSICT hydrogels with different H_2O/HFIP ratios. The hydrogels, from left to right, correspond to samples 2 to 9 as listed in Table 1. The hydrogel discs are 20 mm in diameter and 10 mm in thickness. b) Cross-sectional SEM image of freeze-dried BSICT-SF hydrogel of sample 4. c) Cross-sectional SEM image of freeze-dried BSICT-SF hydrogel of sample 8. d) The visual image of the BSICT-SF hydrogels with various 3D structures. e) The visual image of BSICT-SF hydrogels (sample 4 in Table 1) under compression. Hydrogels were about 7 mm in diameter and 7 mm in height. f) Digital photo of a 2 mm-thick BSICT-SF hydrogel film. g and h) Digital photo of a 3 mm-thick (g) and 1.5 mm-thick (h) BSICT-SF hydrogel tube. The inner diameter and thickness of the tubes are 1.0 mm and 0.5 mm, respectively. i) The combination of snapshots of a BSICT-SF ball (sample 4) under intuitive resiliency tests. The diameter of the ball is 38 mm. The image is reconstructed from video snapshots. The snapshots were extracted from the video with a time resolution of ~0.05 second and then arranged sequentially from left to right to obtain the reconstructed image.

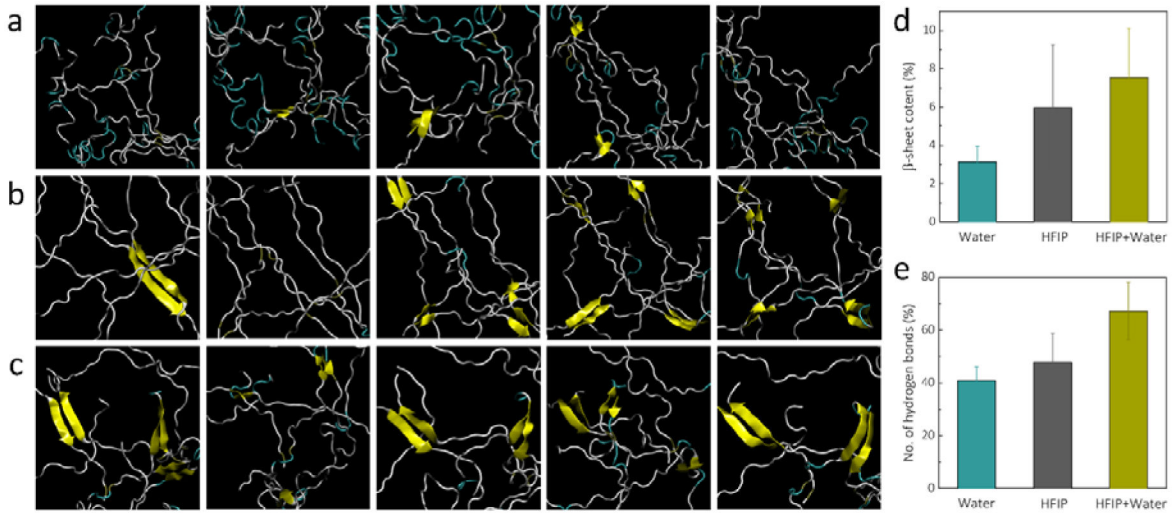

Figure 3.

REST simulations. a-c) Cartoon representations of the top five most populated clusters after REST in explicit a) water, b) HFIP, and c) HFIP/water solvent, where yellow ribbons depict the presence of β-sheets. d and e) Increasing percentages of d) β-sheets and the number of e) hydrogen bonds associated with processing silk in different solvents.

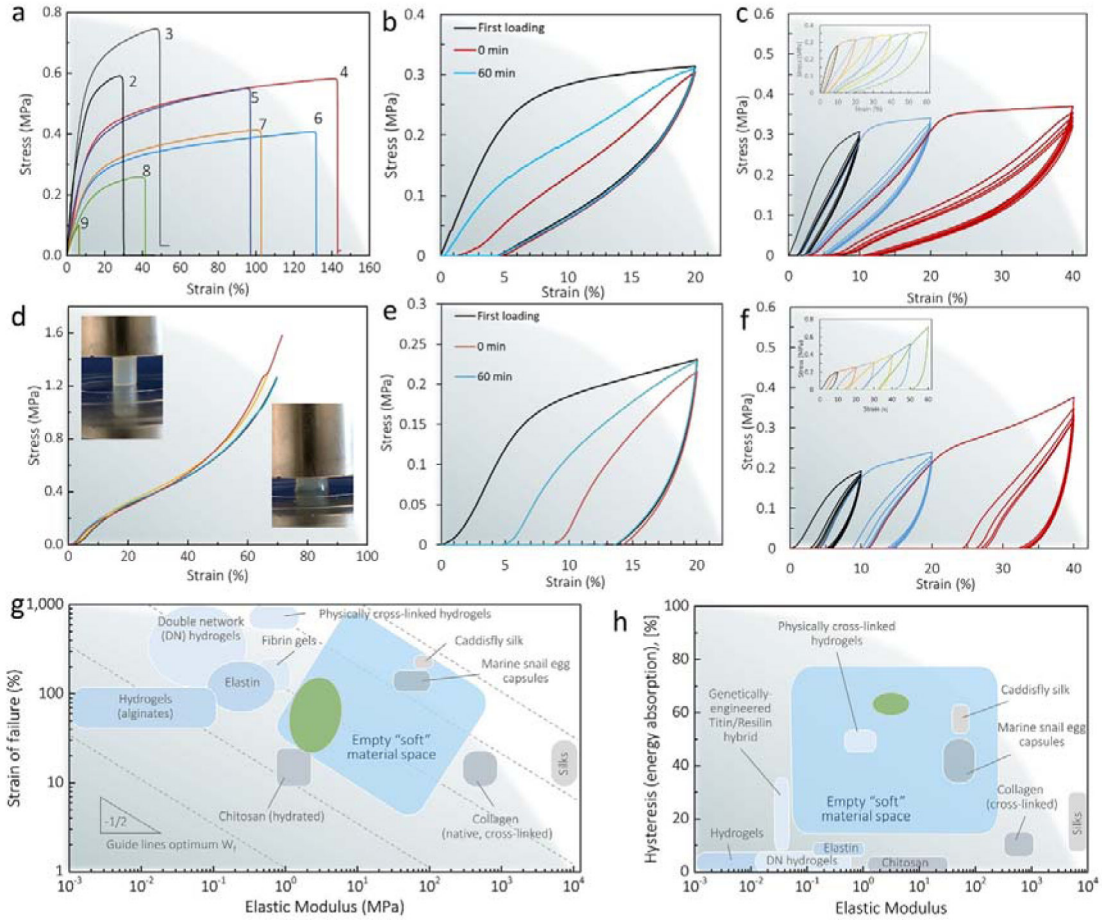

Figure 4.

Mechanical properties of BSICT-SF hydrogels. a) Representative tensile stress-strain curves of BSICT-SF hydrogels. Self recovery test of BSICT-SF hydrogel (sample 4, Table 1) under b) tensile and e) compressive loading. The stress-strain curve of BSICT-SF hydrogel (sample 4 in Table 1) under cyclic c) tensile and f) compressive loading and unloading tests. d) The compressive stress-strain curves of BSICT-SF hydrogels (sample 4 in Table 1). Insets are digital photos of BSICT-SF hydrogel before (top left) and after (bottom right) the compression test. g) Ashby plot of failure strain vs. elastic modulus of BSICT-SF hydrogels and representative soft biomaterials. The Ashby plot of representative soft biomaterials is adapted from ref (56). The dotted lines denoting the guidelines along which materials exhibit an equivalent strain energy to failure.[56] The green area represents the BSICT-SF hydrogels. h) Ashby plot of total hysteresis vs. elastic modulus of BSICT-SF hydrogels and representative soft biomaterials. The Ashby plot of representative soft biomaterials is adapted from ref (56). The blue areas in (g) and (h) correspond to the "empty soft materials space" proposed by Miserez *et al.*[56] The green area represents the BSICT-SF hydrogels. Silks refer to spider dragline silks and *B. mori* silks.

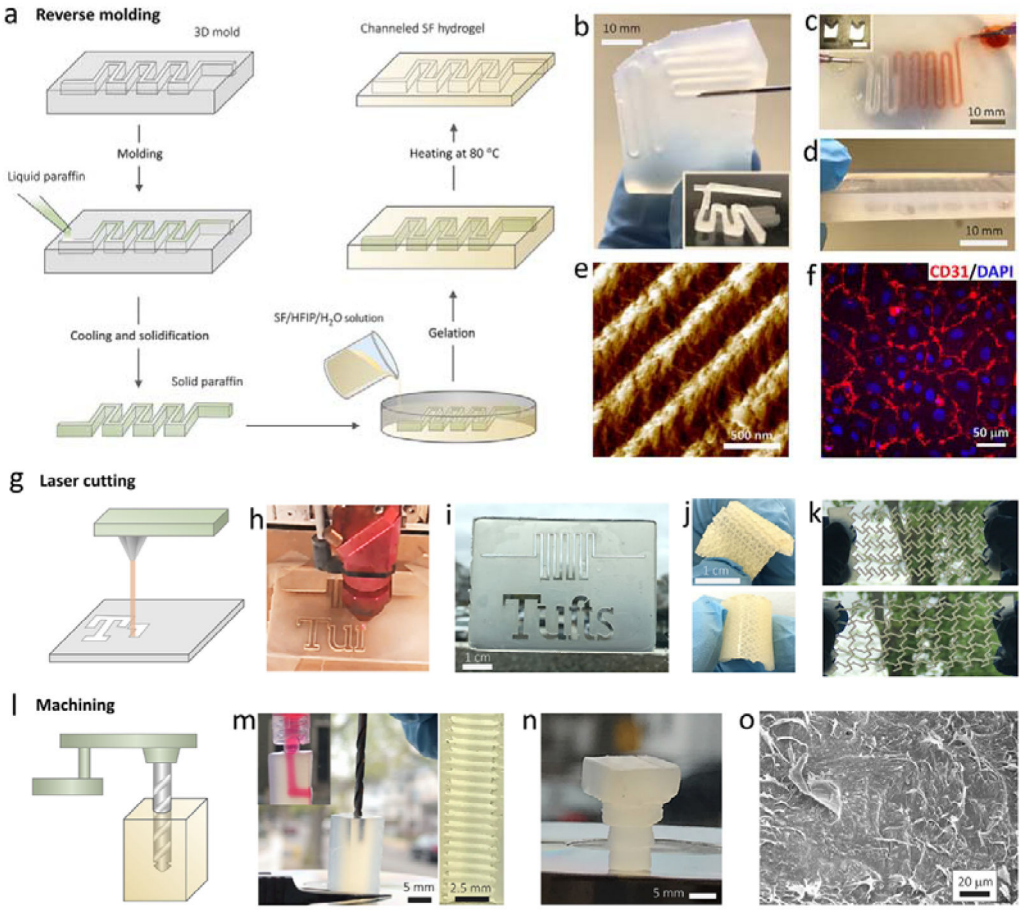

Figure 5.

Universal processing capabilities of BSICT-SF hydrogels. a) The scheme of reverse molding route to produce channeled hydrogels. b) 2D channeled hydrogel. The insert image is the optical microscopy image of channels in the hydrogel. c) 3D channeled hydrogel. The insert image is the photograph of the 3D paraffin pattern used for producing 3D channel. d) The cross-section of the hydrogel that prepared by sequential deposition of three hydrogel layers. e) AFM image of hydrogel pattern of ~450 nm gratings generated via micro/nanomolding. f) Confluent HUVEC cell layer formed on patterned BSICT-SF hydrogels of ~450 nm gratings. g) The scheme of the laser cutting of hydrogel. h) The photograph of the hydrogel during the laser cutting. i)The laser-cut hydrogel with penetrating patterns. j) The laser-cut hydrogel with semi-closed patterns. k) The auxetic deformation of a reentrant honeycomb BSICT-SF hydrogel fabricated by laser cutting. Top image, the hydrogel before stretching; bottom image, the hydrogel after stretching. l) The scheme of the machining of the hydrogel. m) The photograph of the machining of the bulk hydrogel by using drill bit. The top insert image is the dye solution pass through the machined channel. The right image is the photograph of the inner sawtooth structures of hydrogel channel created by machining. n) The machined hydrogel screw. o) SEM image of the surface of the hydrogel screw. All of the hydrogel constructs were produced from hydrogels of sample 4.

Table 1.

The composition, gelation time, structures and physical properties of BSICT-SF hydrogels.

Sample	Dosage of SF and solvent[a]			Percentage of each component			Gelation time[b] (days)	SF/water content of hydrogel (wt%)	Structure and physical properties of hydrogel	
	Water (ml)	HFIP (ml)	SF (g)	Water (wt%)	HFIP (wt%)	SF (wt %)			β-sheet content[c] (%)	Transmittance at 800 nm[d] (%)
1	0.6	3	0.45	10	82	8	> 10	--	--	--
2	0.9	3	0.45	15	78	7	> 5	14.0±0.4/86.0±0.4	35±1	90
3	1.2	3	0.45	19	74	7	3	11.0±0.3/89.0±0.3	35±1	88
4	1.5	3	0.45	22	71	7	2	10.6±0.1/89.4±0.1	37±1	89
5	1.8	3	0.45	26	68	6	2	10.7±0.3/89.3±0.3	36±2	76
6	2.1	3	0.45	29	65	6	1	10.0±0.1/90.0±0.1	35±4	73
7	2.4	3	0.45	31	63	6	1	9.2±0.3/90.8±0.3	35±1	67
8	2.7	3	0.45	34	60	6	1	8.7±0.2/91.3±0.2	35±1	55
9	3.3	3	0.45	39	56	5	1	8.3±0.3/91.7±0.3	35±1	47

[a] In all of these experiments, the desired volume of DI water was dropped into 3 ml 15% w/v SF/HFIP solution.

[b] The gelation (sol–gel transition) time was determined by inverted tube test.

[c] The β-sheet content was estimated from deconvolution of amide I band of freeze-dried BSICT-SF hydrogels.

[d] The transmittance of 400-μm-thick BSICT-SF hydrogels at 800 nm was determined by a fiber-optic spectrometer. The detailed measurements of gelation time, porosity, β-sheet content and transmittance of BSICT-SF hydrogels can be found in the methods.